Aerodynamic Performance Assessment of an Airfoil at Reynolds Number 10000: A Computational Approach

J. Navya Teja[1], Aslesha Bodavula[2], Govardhan Dussa[3]

[1] *M. tech student, Institute of Aeronautical Engineering, Dundigal, Hyderabad, Telangana.* navyateja98@gmail.com
[2] *Assistant professor, Institute of Aeronautical Engineering, Dundigal, Hyderabad, Telangana.* asleshabodavula@gmail.com
[3] *Professor, Institute of Aeronautical Engineering, Dundigal, Hyderabad, Telangana.* dussagovardhan@gmail.com

Abstract: Effects of a low Reynolds number flow on an airfoil with cavities of a specified shape are analyzed computationally to assess the aerodynamic performance by observing the coefficients of lift and drag with increasing angles of attacks. The Reynolds number considered for the simulation is 1×10^4 operating at atmospheric conditions at sea level. Indentations with a definite shape (right-angled triangle) are utilized to find the vortex effects of air in the cavity on the shear layer separation on airfoil surface to retain the flow even at higher angles of attack. The simulation is run in ANSYS Fluent to study the increase in the aerodynamic performance, research findings include an increase in coefficient of lift values by approximately, 111.86% of cavity with depth 0.05C indented at 70% of the chord length at 6° angle of attack, 68.13% of cavity with depth 0.05C indented at 50% of chord length at 6° angle of attack, 23.93% of cavity with depth 0.025C indented at 70% of chord length at 6° angle of attack, 3.96% of cavity of depth 0.025C at 6° angle of attack, 9.59% of cavity of depth 0.05C at 18° angle of attack.

Keywords: Cavity, Airfoil, NACA-0012, Reynolds number, CFD simulation

NOMENCLATURE

C_l = Lift coefficient
C_d = Drag coefficient
α = Angle of attack
C = Airfoil chord length, m.
C_p = pressure coefficient
F_1 = blending function in the shear-stress transport model
k = turbulent kinetic energy, m^2/s^2
L = length, m
N = amplification factor
P_k = turbulent kinetic energy production rate, $kg/m \cdot s^3$
p = pressure, $kg/m \cdot s^2$
Re = chord-based Reynolds number
Re_θ = momentum-thickness Reynolds number, $\rho\theta U/\mu$
$Re_{\theta t}$ = freestream transition-onset momentum-thickness Reynolds number, $\rho\theta_t U/\mu$
$\tilde{Re}_{\theta t}$ = local transition-onset momentum-thickness Reynolds number, $\rho\theta_t U/\mu$
Re_v = strain-rate Reynolds number
S = strain-rate magnitude, $2(S_{ij}S_{ij})^{0.5}$; strain-rate tensor, $0.5(\partial U_j/\partial x_j+\partial U_j/\partial x_i)$
Tu = turbulence intensity, $100(2k/3)^{0.5}/U$
t = time, s
U = freestream velocity, m/s
u = local velocity, m/s
γ = intermittency
θ = momentum thickness, m
μ = dynamic viscosity, $kg/m \cdot s$
μ_t = eddy viscosity, $kg/m \cdot s$
υ = kinematic viscosity, μ/ρ, m^2/s
ρ = density, kg/m^3
τ_w = wall shear stress, $kg/m \cdot s^2$
ω = turbulent eddy frequency, s^{-1}
η = Efficiency

1. INTRODUCTION

The flow characteristics at Reynolds number 10^4 are mostly considered to be a low Reynolds number flow, such flows have more chances of causing shear layer transition, leading to an early separation of boundary layer. The surface adhering properties of fluid over body tend to minimize and the flow separates, for an airfoil subjected to such flow may cause stall due to turbulent flow over the surface, as the direction of the fluid flow increases. The flow over an airfoil in different conditions has been studied by many researchers, and low Reynolds number flows have been researched upon. Modifications done to the surface of the airfoil is being tested both physically and computationally to produce useful solutions for improving the operation of these. These simple modifications may help in avoiding the problems faced by modern-day aircraft, attaining flight in different conditions with rapid flow changes. The lift and drag

coefficients of each airfoil at different angles of attack are analysed. The findings would provide valuable insights into the efficiency of these airfoils' low Reynolds number flows. This may help inform and reform the design of aircraft for future aircrafts. Low Reynolds number flow analysis done by Joshua N. N. Counsil for the airfoil NACA 0012 at Reynolds number 10^5 for the airfoil specifying in detail the effects of flow over two different airfoils and a flat plate with the solution adapting to the γ-Re_θ model of Shear Stress Transport equations, as a comparison for determining the efficient one among the both airfoils [1], this helped select an optimum airfoil to study the performance characteristics. Al Habib Ullah proved both computationally and experimentally that indentations influence the airflow on the body of the airfoil using Particle Image Velocimetry (PIV) [2]. Eric. C Miller proved that increasing the depth of the indentations results in extending the boundary layer by using the PIV method [3]. This helped select different depths for the same cavity type for the aerodynamic performance analysis. However, the type of profile and the type of depth of a cavity is purely a logical approach to studying the effects of the airflow around the airfoil and how the cavities contribute to it. A PIV study done by Adam Stolt included placing the hemispherical cavity matrix at the leading edge of the airfoil body [4], this helped gain insights on the locations for the cavities to be placed on the surface of the airfoil, as the study suggested placing a number of dimples all over the leading edge was a downgrade to the airfoil performance, which helped select another location on the airfoil farther than 20% of chord length. PIV study done by Yan Zhang dealt with modifying the airfoil with cavities and protrusions including three different types of modification on the airfoil surface [5], the study proved out the cavities placed all along the leading edge of the airfoil body till 20% of the chord length is not an effective solution, whereas the protruded surfaces of airfoil proved out to be better performance enhancing than airfoil with dimples, this helped gain valuable insight on the location of protrusion placed on the body of airfoil.

For a deeper understanding of the vortex movements in the dimple region Wang. Z studied the vortex flow in a dimpled depression and the vortex effects. The typical shape of the vortex with the flow, fully computationally, although many authors prefer studying the effects of dimples or depressions and the change caused by the flow around the body due to it. The flow in the dimple region itself proves out to be a greater approach to understanding the flow around the dimple and on the dimpled surface. Here the vortex type and shape are in a horseshoe-like shape and in a straight line [6]. Vortex frequency CFD simulation done by Robert C. Vincent proved that the depth of a cavity and the boundary layer both have an influence over the flow parameters over a dimple. The depth of the cavity as increased produces a prolonged effect on the vortex generated. The bigger the vortex, lower the boundary layer separation. Physical experimental setup of the former helped attain highly accurate results. Similarly, the computational methods having a greater chance in attaining closer results to that of the experimental ones [7].

The surface flow analysis done by Olaf W.G van Campenhout gave more information on the three-dimensional flow around the body with indentations, it was observed to be a converger-diffuser type flow topology indicated clearly by the velocity streak-lines [8]. The investigation on active dimple behavior done by Natalie Udovchik, helped understand the effect of increase in the dimple depth in the flow around the body of the surface, the flow altered as the depth changed, the cavity is of a cylindrical type equipped with mechanical controls to simultaneously increase and decrease the depth of the cavity [9]. Active dimple with frequently changing dimple ratio basing on the dimple depth changes done by Junki Hamada, to be a ratio of diameter of the circular cavity and depth of the cavity, the frequency of changes in the ratio when altered correctly provided good resistance to induced flow over the surface being tested, it provided valuable insights in choosing the depth of the cavity [10]. As the shapes of the dimples have been examined on the account of drag-reducing characteristics. An optimum shape of a dimple is yet to be determined, designed and researched by authors who have already researched the vortex shape of the airflow vortex, around the airfoil. Also, an in-detail study of the vortex zones on the 3-dimensional space of the dimple body. Making necessary surface modifications to the dimple's 3-dimensional structure can be utilized as a supportive measure to improve the overall flow over the dimpled surface. Cumulative research on whether a cavity with an asymmetric shape and structure can be researched upon by researchers. The different types of non- axisymmetric bodies can be treated as differently modified cavities serving different purposes on the body of the surface subjected to the flow. An axisymmetric body would tend to give a type of effect which has proved to be a good alternative to different shapes [11].

Tay Chien Ming Jonathan studied the effects of different shaped dimples or indentations comprising teardrop and diamond-shaped dimples. These are placed in a matrix of shapes with gaps and with their central axis aligned in the direction of the flow on the surface of the airfoil. The simulation was carried out with sea level atmospheric conditions

and the teardrop-shaped dimples proved to be comparatively best in drag reduction. The usage of different shaped dimples in the form of a matrix of a number of shapes occupying different locations. Creating a pattern has provided new insights on the working of dimples on the surface indented with them. The continuation of the surface after the dimple surface ends. A matrix of different shapes has proved out to have a better impact on boundary layer separation and drag characteristics [12,13]. Protrusions provide the same effect as that of a dimple. When compared to dimples protrusions have less contribution in drag reduction and shear layer separation on top of the surface of the body. Protrusions have less effect on boundary layer separation when compared to the plain airfoil without any protrusions or dimples [14,15,16]. The indentations or dimples have proven to have a good contribution in reducing the shear layer separation on the surface of the airfoil at higher angles of attack. Although many researchers have attempted to use different types of indentations of different sizes, depths, and placement types, both above and below a surface, to summarize this, the depths of a single type of cavity can be tested on different regions of an airfoil surface. Numerical investigation done on the triangular cavity type by Bodavula A, helped gain valuable insights on the effect of adding either cavity and protrusions on the cavity on the airfoil body also helped choose a pre-existing design for the test airfoil [17,18,19]. Provided the research on the solver model done by the former, which employs transition Shear Stress Transport equations to stabilize the solution with the transport equations, this is deemed as an efficient method for getting accurate results in a fluid simulation [20,21]. Studying airfoil with NACA 0012 profile to determine the drag characteristics also provided valuable insights helping ease the understanding on behavior of airfoil protrusions in different angles of attacks at different fluid flow properties [22].

The learnings from the aforementioned researchers have provided valuable information on dimpled surfaces. The characteristics of flow as the dimple shape and depth change, and the effects of dimple shape on the flow over an airfoil. These quantities and factors can be readily studied with a numerical investigation at different conditions. Out of which the Reynolds number 10^4 is considered, as the flow may cause stall at low angles of attack. The aim and purpose of the research is to find and prove diverse ways of improving airfoil performance with enhancements and modifications to the airfoil surface. A computational approach with optimized refined solution and method to prove and justify the approach. This paper focuses on a numerical investigation of airfoil performance for low Reynolds number flows. The study utilizes computational fluid dynamics (CFD) simulations to analyze the lift and drag characteristics of an airfoil (NACA 0012) under a specified Reynolds number flow condition ($Re=10^4$). Specifically, a numerical investigation of the effects of cavities on the airfoil surface to improve the flow around the airfoil is done.

2. METHODOLOGY

A. Numerical Method

Numerical methods are the mathematical approach of the research to replicate the physical phenomenon into a computable system. The software used here is ANSYS Fluent, which has a set of predefined equations. Signifying the different flow physics to help analyse and simulate the flow of fluids with varying mechanical properties.

1) Equations

ANSYS Fluent uses the below mentioned Navier – Stokes Equation as the main equation for solving the problem

$$\frac{\partial \rho}{\partial t} + \frac{\partial}{\partial x_j}\left(\rho U_j\right) = 0 \tag{1}$$

$$\frac{\partial}{\partial t}\left(\rho U_i\right) + \frac{\partial}{\partial x_j}\left(\rho U_j U_i\right) = -\frac{\partial p}{\partial x_i} + \frac{\partial}{\partial x_j}\left[\mu_{eff}\left(\frac{\partial U_i}{\partial x_j} + \frac{\partial U_j}{\partial x_i}\right)\right] \tag{2}$$

A control volume-based finite element method is employed to discretize these equations. The spatial discretization utilizes a hybrid scheme that combines first- and second-order accuracy. This scheme dynamically transitions from the second-order scheme to the first-order scheme in areas with pronounced spatial gradients. In terms of accuracy, the scheme with a higher resolution is formally accurate to first order in space. However, in practical terms, it achieves an approximate spatial accuracy with second order. The coupling with pressure-velocity using a grid which is non staggered and the algorithm with the accurate Rhie and Chow fourth-order equation. The discretization is achieved through Euler scheme having a second order which are backward and implicit equations, utilizing iterative process. In the inner loop the coefficients are calculated and updated, provided the outer loop focuses mainly on the time

advancement of the solution. To enhance the efficiency and check the performability, a collection of decomposition of the domain and a processing which applies parallelly over a local region around the two partitions is utilized, along with a solver consisting coupled equations with solver at multiple grids algebraically and an effective frequent information exchanging working interface in between the different partitions. The Shear Stress Transport equation model is based on the following equations, which also enact as the transport equations.

$$\frac{\partial(\rho k)}{\partial t}+\frac{\partial(\rho U_j k)}{\partial x_j}=P_k-\beta^*\rho k\omega+\frac{\partial}{\partial x_j}\left[(\mu+\sigma_k\mu_t)\frac{\partial k}{\partial x_j}\right] \quad (3)$$

$$\frac{\partial(\rho\omega)}{\partial t}+\frac{\partial(\rho U_j\omega)}{\partial x_j}=\alpha\rho S^2-\beta\rho\omega^2+\frac{\partial}{\partial x_j}\left[(\mu+\sigma_\omega\mu_t)\frac{\partial k}{\partial x_j}\right]+2(1-F_1)\rho\sigma_{\omega 2}\frac{1}{\omega}\frac{\partial k}{\partial x_j}\frac{\partial\omega}{\partial x_j} \quad (4)$$

The value of F_1 usually assumed to be zero outside the observable surface in the k-ε model, indicating that it no more helps achieve change of any sort in the solution. In the subsequent separation of the shear layer in the k-ε model, F_1 is set to 1, signifying its full effect on the solution. The distance in between the separation layer and the wall is computed by solving a Poisson equation, this shares frequent compatibility with modern Computational Fluid Dynamics (CFD) defined codes. The γ-Re_θ model of the Shear Stress Transport equations in fluent are predominantly based on the Reynolds number consisting momentum thickness properties [23]. The Reynolds number mentioned shares a direct proportionality with the Reynolds number having maximum strain rate, facilitating an advantage by being a calculatable property at each specified grid point locally.

$$Re_\theta=\frac{\max(Re_v)}{2.193};\ Re_v=\frac{y^2S}{v} \quad (5)$$

Two more transport equations are utilised, each of them for Reynolds number having transition momentum thickness and intermittency over the surface:

$$\frac{\partial(\rho\gamma)}{\partial t}+\frac{\partial(\rho U_j\gamma)}{\partial x_j}=P_\gamma-E_\gamma+\frac{\partial}{\partial x_j}\left[\left(\mu+\frac{\mu_t}{\sigma_\gamma}\right)\frac{\partial\gamma}{\partial x_j}\right] \quad (6)$$

$$\frac{\partial(\rho\check{R}e_{\theta t})}{\partial t}+\frac{\partial(\rho U_j\check{R}e_{\theta t})}{\partial x_j}=P_{\theta t}+\frac{\partial}{\partial x_j}\left[\sigma_{\theta t}(\mu+\mu_t)\frac{\partial\check{R}e_{\theta t}}{\partial x_j}\right] \quad (7)$$

The transport equation regarding intermittency is employed to determine the initiation of transition (when γ > 0). On the other hand, the transport equation for the momentum-thickness Reynolds number indicates the location of transition onset and captures the nonlocal influence of freestream-turbulence intensity and pressure gradient at the edge of the boundary layer [24]. In Equation (6), the source term Pγ is designed to be zero in the laminar boundary layer before the transition occurs and becomes active whenever the local strain-rate Reynolds number surpasses the local transition-onset criterion. The destruction source term E_γ is designed to ensure that the intermittency remains close to zero in the laminar boundary layer. It allows for the prediction of re-laminarization when the transition-onset criterion is no longer met and becomes negligible in the fully turbulent regime. The purpose of Equation (7) is to utilize a correlation to calculate the Reynolds number based on momentum thickness ($Re_{\theta t}$) in the freestream and enable the diffusion of this freestream value into the shear layer. The aforementioned term $P_{\theta t}$ takes care such that the value of $\check{R}e_{\theta t}$ shares a significant match with $Re_{\theta t}$ value which is dependent on the correlation outside the shear layer and gets deactivated within the shear layer [25,26].

B. Clean Airfoil mesh generation

NACA0012 airfoil of 1m chord length is elongated by 8mm to give a sharp trailing edge to the airfoil. The domain is a C-type domain with domain size 20C acting as a factor of the chord length [1]. The Simulations are run for the airfoil without any depressions, at different angles of attacks to replicate the Computational values from the base paper [1]. The simulation has been run for mesh having elements 100,000 to 300,000, after 250,000 the values

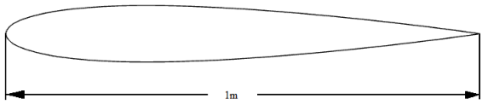

Fig. 1. NACA-0012 airfoil of 1m chord length.

match with each iteration of mesh generation, hence the grid independent study is achieved. The Solver setup used for the solution is primarily using the γRe-θ transition SST 4-equation model. With enhanced relaxation factors to facilitate the increased stability in the solution for C_l and C_d values of the airfoil, at different angles of attack. The preferred method is a simple scheme with second-order equations for the mechanical properties of the fluid. The simulation is run for Re = 1×10^4. The primary aim of doing this is to increase the grid independency of the airfoil C_p Vs X/C graph for a particular angle to study the influence of the increase in the number of elements in the mesh for the values in a grid. The values matched with those indicated in the paper [1]. The solver is validated successfully, and the same process is repeated for an airfoil of the same length with the same solver setup at low Reynolds number flow such as Re = 1×10^4 the values of C_l and C_d are recorded for comparison with the airfoils with cavities indented.

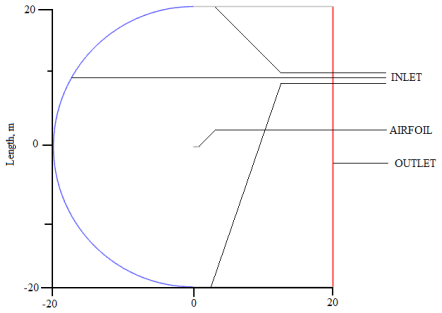

Fig. 2. Dimensions of the domain created for clean and cavity airfoils with boundary conditions.

C. Cavity indented Airfoil test

The NACA 0012 airfoil with a 1m chord length is given an 8mm increase in length at the trailing edge. It is then equipped with a right-angled triangle-shaped depression with the wedge facing the trailing edge. Designed to facilitate the buildup of a vortex in the cavity and support a smooth transition of boundary layer to the trailing edge. The wedge is faced towards the trailing edge to prevent any vortex buildup at the exiting layer of the flow. The depth of the cavity is determined by the chord length of the airfoil. With two cavities of different depths considered, one measuring 0.025 of the chord length and the other measuring 0.050 of the chord length. The analysis involves placing the three cavities at different locations on the body of the airfoil, specifically at 30%, 50% and 70% of the chord length (C).

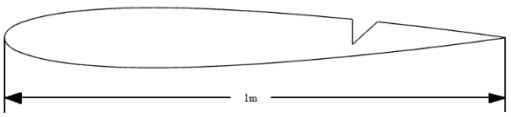

Fig. 3. Airfoil profile with the triangular indentation 0f depth 0.05C at 70% of chord length.

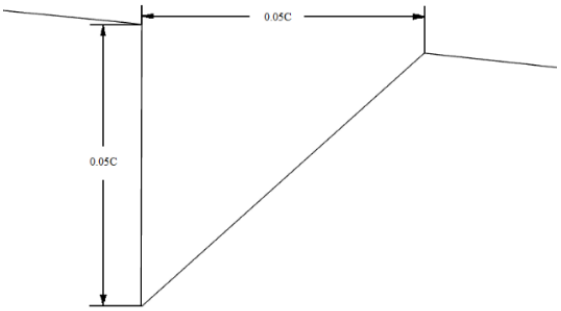

Fig. 4. Dimensions of the indentation with a depth of 0.05C.

The mesh created is similar to that of the clean airfoil, with a radius of 20C and an extended length of 20C along the trailing edge of the airfoil. Mesh lines are divided more on focusing over the airfoil to achieve maximum accuracy in the Coefficients of both lift and drag of the airfoils. It is often considered that the mesh has a zone of concentrated mesh elements to maximize the accuracy. However, placing the zone as near to the airfoil as possible has proven to increase the quality as well as the mesh orientation.

The simulation is performed using ANSYS Fluent, with atmospheric conditions modeled after those on Earth at sea level. A fluid velocity of 0.150 m/s, and a Reynolds number flow of 1×10^4. The simulation assumes a fluid density of 1.227 kg/m^3, a temperature of 288 K. The fluid properties are basic fluid air preset in ANSYS Fluent materials. The simulation utilizes a γRe-θ transition SST model simple scheme with Rhie and Chow distance-based second-order upwind equations to study the behavior of the NACA 0012 airfoil with the cavities until it reaches stall at higher angles of attack. The cavities have been found to improve fluid adherence to the airfoil even at higher angles of attack, with lift and drag coefficients providing valuable insights into the airfoil's aerodynamic performance.

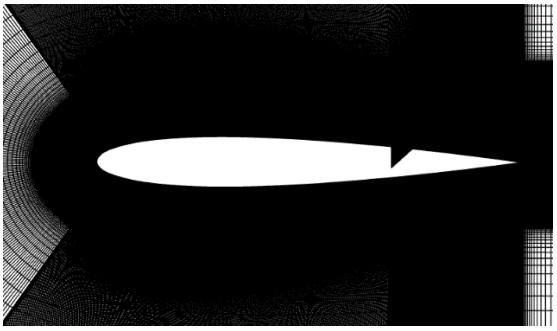

Fig. 5. The meshing around the cavity and airfoil.

3. RESULTS AND DISCUSSION

The simulation was carried out for all the airfoils at different angles of attack changed using the component values, the angle of attack varying from 0° – 20°. As the angle of attacks changed there was a gradual change in C_l values, and a substantial increase in the Coefficients of drag and lift compared to the ones of airfoil without indentations. Although the Coefficients of Lift and drag provide clear information on the behavior of NACA-0012 of chord length 1m in Re=10^4. The flow has fewer distortions when compared to lower angles of attacks and the flow separation occurs at expected regions, the indentations proved to have provided a substantial increase in Lift and Drag at lower angles of attack such as 4°, 6°, 8° and 10°. The change caused in the lift and drag properties of the airfoil has been given below in a graphical form depicting the change in the coefficients with the change in the angle of attack of the flow direction.

The turbulence intermittency contour shows a thick transition layer on the surface of the NACA 0012 airfoil. Constituting effectiveness of the simulated air flowing over it at Reynolds number 10^4 and the vortexes building up at the region almost near 30% of the chord length of the airfoil body. Cavities with 0.025C of depth have a good response to turbulence. The velocity streamlines have been distributed evenly on the surface of the airfoil. Facilitating a matrix

of vortexes contributing in evenly disturbing the flow over the surface or causing little disturbances and vortexes at a higher angle of attack. It is observable in the comparison C_l and C_d graphs that the drag is decreased in airfoils with cavities of depth 0.025C at the regions 50% and 70% of chord.

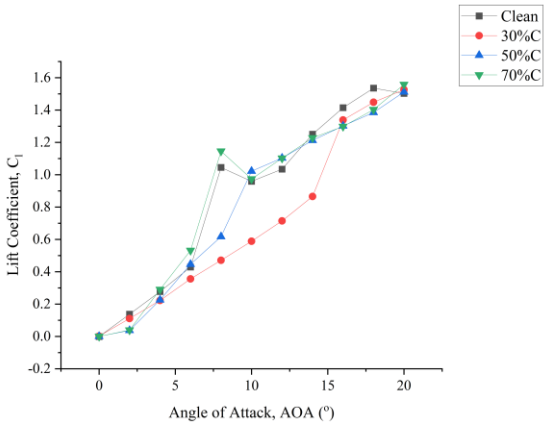

Fig. 6. Coefficient of lift of airfoils with 0.025C depth at three different positions, compared to clean airfoil.

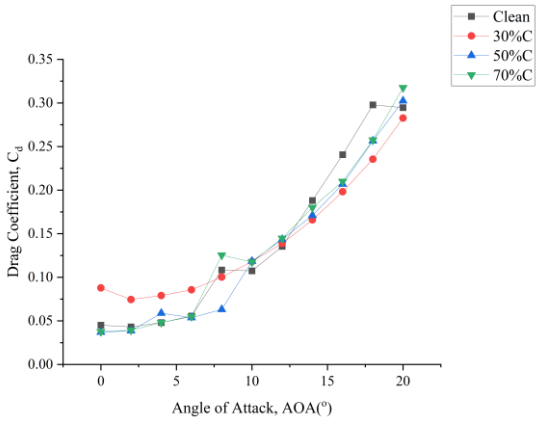

Fig. 7. Coefficient of drag of airfoils with cavity of 0.025C depth at different positions compared to clean airfoil.

However, the cavity placed at 30% of the chord has proven to result in more drag than the former two regions of the cavity. Provided outnumbering even the clean airfoil with a substantial increase in drag at lower angles of attack. This is due to the obstruction created by the cavity and the vortex generated at different angles of attacks.

The efficiency of airfoils compared are shown below as the Angle of attack increases, the efficiency has been observed to increase predominantly. Following the intention, adding a cavity nearer to the leading edge has proved to decrease the efficiency in the initial angles of attack. The cavity indented at 30% of the length of the airfoil body gave very less performance as the lift was decreased due to drag caused by the vortex buildup in the cavity. Due to the vortex buildup at zone nearer to the body the drag characteristics have pertained to increase. This helps in understanding the flow around the airfoil with a cavity at 30% of the chord of the airfoil. Not being an effective solution to increasing the performance of the airfoil.

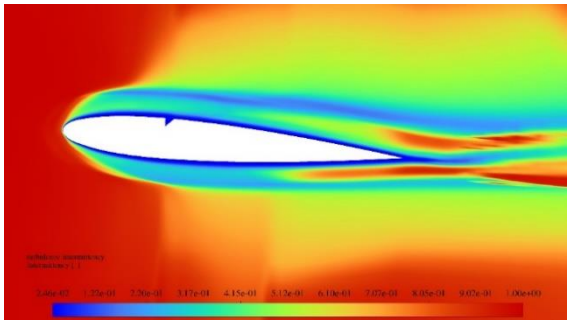

Fig. 9. Transition over the airfoil body, with a cavity of 0.025 of chord-length depth, located at 30% of chord-length and the flow at Reynolds number 10^4, at an angle of attack of 8°.

The same depth cavities placed at different regions have contributed to increasing the performance. Predominantly with 70% of the chord being the optimum region for placing a cavity of depth 0.025C. The flow around the airfoil is a low Reynolds number flow, Re = 10^4. Such flows tend to cause stall at lesser angles of attacks, compared to higher Reynolds number flow. The aforementioned modification has served to increase the efficiency of the airfoil. This can be observed in the C_p vs X graphs showing the change in coefficient of pressure along the body of the airfoil.

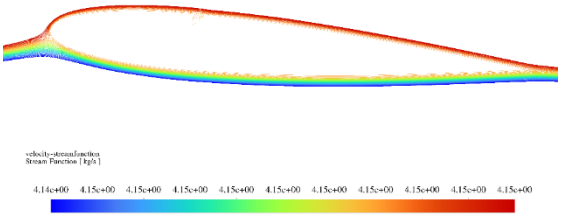

Fig. 8. Streamlines of vortex inside the cavity of depth 0.025C, at 30% of chord-length, and flow at Reynolds number 10^4 and AOA 8°.

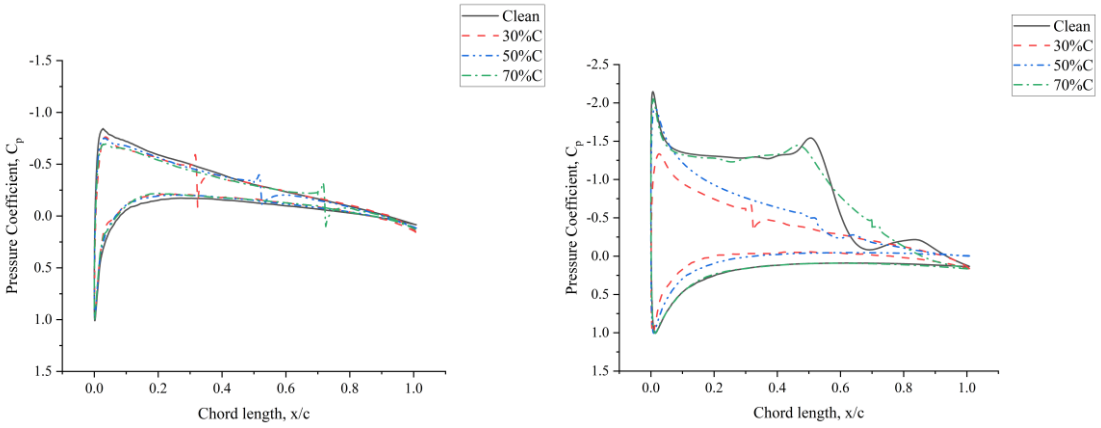

a) C_p vs X at 4°, Re = 10^4

b) C_p vs X at 8°, Re = 10^4

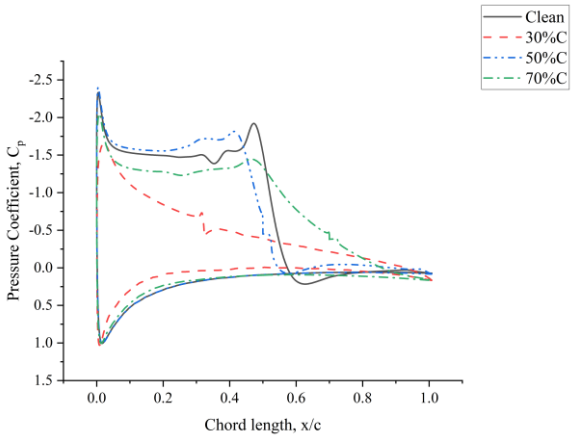

c) C_p vs X at 10°, Re = 10^4

Fig. 10. C_p vs X graphs of airfoils indented with 0.025C placed at different locations at 4°,8° and 10° Angles of attacks at Re = 10^4 comparison with clean airfoil.

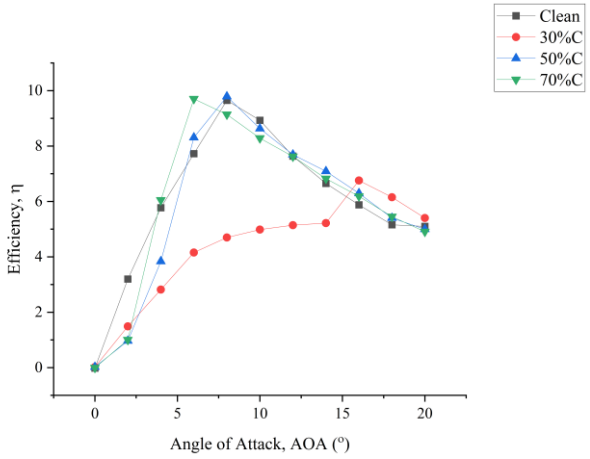

Fig. 11. Efficiency of airfoils with change in angle of attack, having 0.025C depth cavity, at Reynolds number 10^4.

Airfoils with cavities of 0.025C depth placed at 50% and 70% gave a good response in the performance characteristics. They resulted a 9.59% increase in the Coefficient of lift compared to Clean NACA-0012 airfoil with no indentations at 8° angle of attack, and later decreasing gradually to 3% at 20° angle of attack. The vortices generated in the cavity is the main reason behind the sudden performance increase.

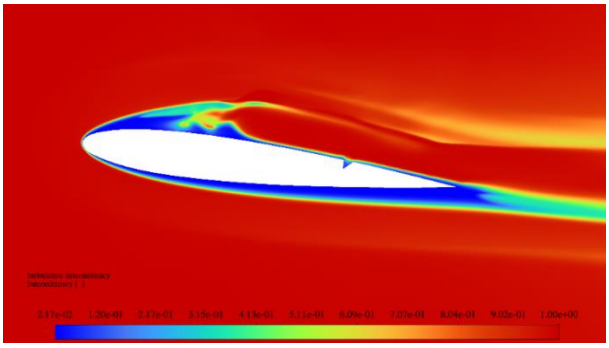

Fig. 12. Transition flow region on the body of the airfoil, with 0.025C indented at 70% of chord at 8° AOA.

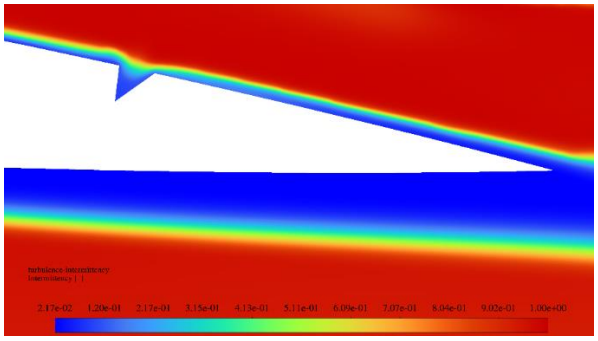

Fig. 13. Transition region of the flow around the cavity.

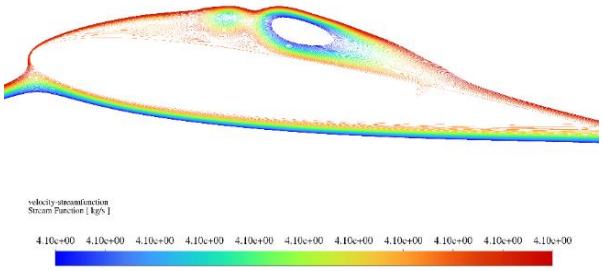

Fig. 14. Streamlines vortexes formed before the cavity, and the flow is completely normal around the cavity.

Cavities with increased depth showed similar results as intended. It was previously understood as the cavities help increase the performance of the airfoils. Increasing the depth furthermore should facilitate vortexes with increased size and operating radius, but the size of the vortexes contributed differently than what was intended outcome. A deeper cavity at 30% chord of the airfoil resulted in increasing the drag characteristics, with a decrease in coefficient of lift by around 53.08% at 8° than the clean airfoil without any indentations and gradually decreasing to 0.32% at 20°, C_l value increased by approximately 9.72% at 18° AOA. Placing a cavity at 30% chord of the airfoil has not supported to be a performance-enhancing modification.

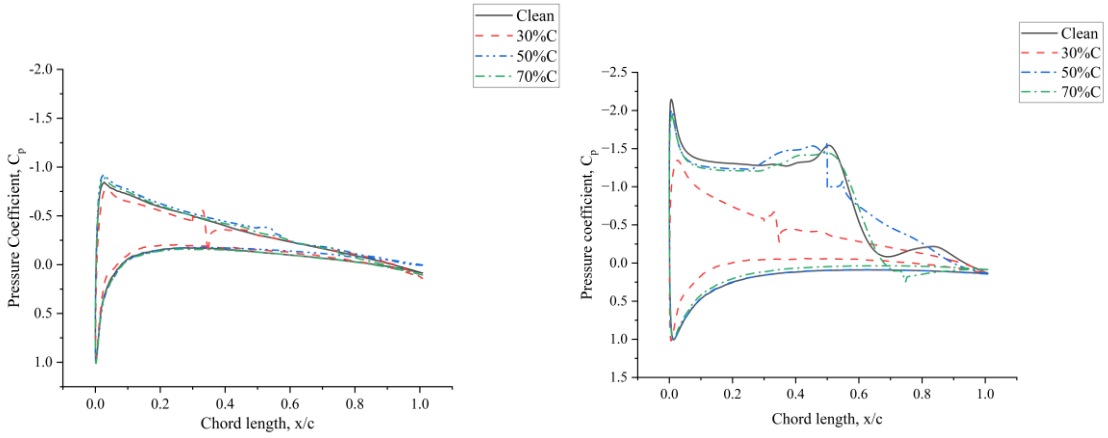

a) C_p vs X at 4°, Re = 10^4

b) C_p vs X at 8°, Re = 10^4

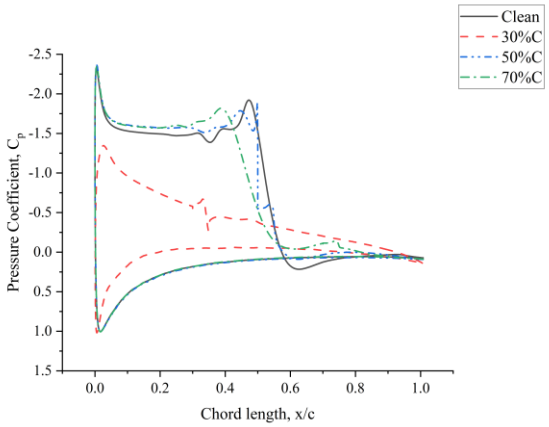

c) C_p vs X at 10°, Re = 10^4

Fig. 15. C_P vs X graphs of airfoils indented with 0.05C placed at different locations at 4°,8° and 10° Angles of attacks at Re = 10^4.

With the decrease in lift, it increased the drag, further decreasing the aerodynamic efficiency. C_p vs X graphs show similar change in pressure coefficient compared to those of the airfoils with indentations of 0.05C. As the coefficient of pressure doesn't have notable change it's the vortexes and rotational flow on top of the surface of the airfoil causing the sudden increase and decrease of C_l and C_d values.

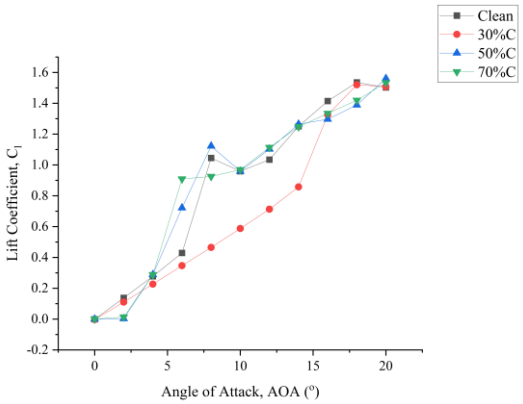

Fig. 16. Coefficient of lift of airfoils with cavity of 0.05C depth at different positions.

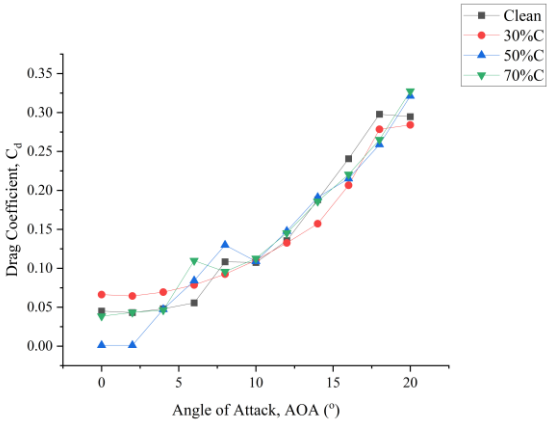

Fig. 17. Coefficient of drag of airfoils with cavity of 0.05C depth at different positions.

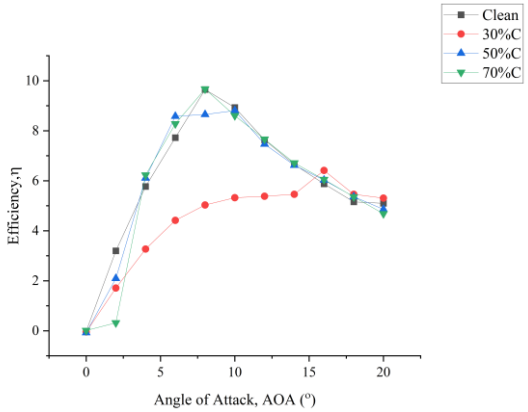

Fig. 18. Efficiency of airfoils with cavity with depth 0.05C at different locations with a flow at Reynolds number 10^4**.**

The efficiency of the airfoils with different depths shows clearly the increase in efficiency with a substantial decrease in drag acting on the airfoil body with the lift increasing gradually. Showing an efficiency peak at an 8° angle of attack. Cavities of depths 0.05C indented at 50% and 70% of the chord have increased performance. Whilst cavity with 0.05C depth indented at 50% of the chord attained a stable increase in efficiency values over 6°, 8°, and 12°, an increase of 68.13%, 7.42% and 6.61% in C_l values respectively.

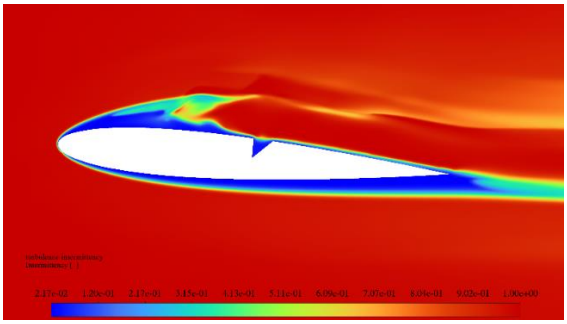

Fig. 19. Transition over 0.05C depth cavity, at 50% Chord at Reynolds number 10^4 at 8° AOA.

The same cavity placed at 70% of the chord, acquired a balance between both C_l and C_d values. Resulted in achieving the peak in aerodynamic efficiency at, 8° angle of attack. With an increase of 111.86%, 1.08% and 7.63% in C_l value at 6°, 10° and 12° AOA, compared to the airfoil without any surface modifications.

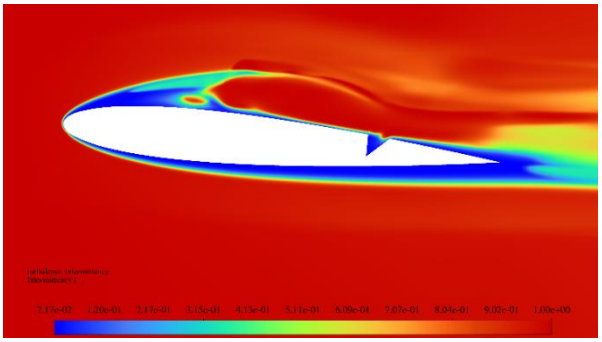

Fig. 20. Transition over airfoil embedded with 0.05C depth cavity at 70% Chord, flow at Reynolds number 10^4 at 8° AOA.

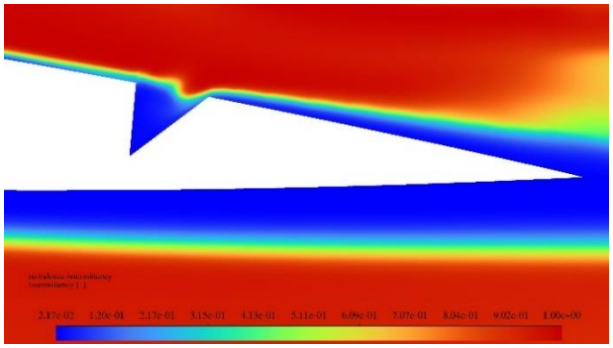

Fig. 21. Transition of flow region around the cavity of depth 0.05C at 70% Chord.

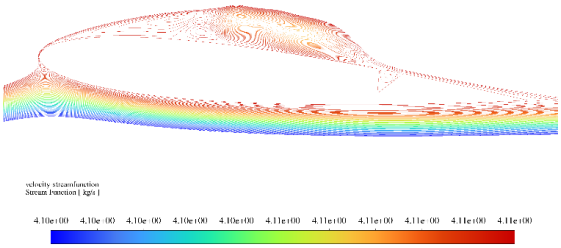

Fig. 22. The vortex and flow streamline around the cavity and the airfoil with 0.05C depth cavity at 70% Chord and 8° AOA.

Increase in the efficiency values of cavity with depth 0.025C located at 70% of chord length, balancing out due to less drag at this AOA. This gradually decreases as the angle of attack moves to 16° and later to 20°, a typical flow behavior is seen, the cavity responsible for vortex creation, becomes main contributor in increasing the drag. Resulting in a reduce in performance. This happened because of the shear layer separation happening due to the cavity at higher angles of attack. Although the performance values suggest the optimum performance and the optimum position to place such a cavity or any other cavity of similar geometry. The reasoning may be validated, but is yet to be experimented with and analysed physically with physical models. The numerical investigation and its results regarding the parameters affecting the flight characteristics and performance of the airfoil will serve as a valuable asset in developing technology, serving the purpose of the research work.

4. CONCLUSION AND FUTURE WORK

The simulation results have succeeded in providing necessary information helping prove the aerodynamic performance of the airfoil with a cavity is much more increased at different angles of attack. With an 111.86% increase in C_l values of 0.05C depth cavity at 70% of chord length, and increased efficiency compared to clean airfoil at 6° AOA at the same angle of attack the cavity of depth 0.05 placed at 50% of chord length showed an increase of 68.13% approximately in C_l value both of them gradually changing and lowering down with increase in AOA. An approximate 3.96% increase in C_l values for cavity with depth 0.025C placed at 50% of chord length at 8° AOA and an increase of 23.93% in C_l values for the same cavity indented at 70% of chord length both at 6° AOA. A 9.59% increase in C_l values of 0.025C depth placed at 70% both at 8° AOA, also at 50% chord both the cavities showed a nominal increase in C_l values. With 0.05C at 70% chord having an increase of approximately 7.42% at 8° AOA. The airfoil with the cavity of depth 0.025 and 0.05 times of chord can be treated as optimum depths for a cavity. The optimum location for placing such cavities on the surface of the airfoil would be around 70% of the chord length. Specifying over different angles of attack, even the efficiency increase is gradual with an increase in the depth of the airfoil. Designing such a wing with such modifications with perfect structural strength to support the aircraft's motion and retain the shape may prove out to be a challenging task to overcome. With more amount of research in this area, an optimum shape of the cavity which also contributes in retaining the wing structure intact and also provides good drag resistance to stall characteristics of an airfoil can be designed and developed.

5. REFERENCES

[1]. Joshua N. N. Counsil, "Low-Reynolds-number aerodynamic performances of the NACA 0012 and Selig–Donovan 7003 airfoils," AIAA journal of aircraft vol. 50, no. 1, pp. 204-216, May 2013.
[2]. Al Habib Ullah, Braden Rostad, Jordi Estevadeordal, "PIV study of the flow interaction between a three-cylinder rotating system and a downstream Dimpled airfoil," AIAA Aviation Forum, June 2019.
[3]. Erik C. Miller, "Effects on boundary layer caused by inclusion of dimples at varying depths," AIAA Journal of aircraft, vol. 49, no. 4, pp. 959-972, Sep. 2012.
[4]. Adam Stolt, Jordi Estevadeordal, JesstinKrech and Yan Zhang, "A tomographic PIV and TSP study of leading-edge structures on stall behaviors of NACA0015," 55th AIAA Aerospace Sciences Meeting, AIAA SciTech Forum, Jan. 2017.
[5]. Yan Zhang, Sadhana Bhusal, JesstinKrech, Jordi Estevadeordal, "Effects of leading-edge structures on stall behaviors of a NACA0015 airfoil: a Multi-Plane PIV study," 34th AIAA Applied Aerodynamics Conference, June 2016.
[6]. Wang Z, Yeo K. S, Khoo B. C, "Numerical simulation of laminar channel flow over dimpled surface," 16th AIAA Computational Fluid Dynamics Conference, (June 2003).
[7]. Robert C. Vincent, Raymond C. Maple, "CFD investigation of laminar flow over a dimpled surface indentation," 36th AIAA Fluid Dynamics Conference and Exhibit, June 2006.
[8]. Olaf W.G. van Campenhout, Michiel van Nesselrooij, Leo L.M. Veldhuis, Bas W. van Oudheusden, Ferdinand F.J. and Schrijer, "An experimental investigation into the flow mechanics of dimpled surfaces in turbulent boundary
[9]. layers," 2018 AIAA Aerospace Sciences Meeting, Jan. 2018.
[10]. Natalie Udovidchik, Jonathan F. Morrison, "Investigation of active dimple actuators for separation control," 3rd AIAA Flow Control Conference, June 2006.
[11]. Junki Hamada, Masahiro Motosuke, Shinji Honami, "Fundamental characteristic of the induced flow by active dimple," 50th AIAA Aerospace Sciences Meeting including the New Horizons Forum and Aerospace Exposition, Jan. 2012.
[12]. Chien M. Tay, Tee T. Lim, "Drag reduction with non-axisymmetric dimples," 35th AIAA Applied Aerodynamics Conference, AIAA Aviation Forum, June 2017.
[13]. Tay Chien Ming Jonathan, Lim Tee Tai, "Drag reduction with teardrop-shaped dimples," 2018 Flow Control Conference, AIAA Aviation Forum, June 2018.
[14]. Tay Chien Ming Jonathan, Lim Tee Tai, and Khoo Boo Cheong, "Drag reduction with diamond-shaped dimples," AIAA Aviation Forum, June. 2019.
[15]. John P. Casey and Paul I. King, "Parameterization of boundary layer control dimples on a low-pressure turbine blade," 40th AIAA/ASME/SAE/ASEE Joint Propulsion Conference and Exhibit, July 2004.
[16]. C. M. Tay, "Determining the effect of dimples on drag in a turbulent channel flow," 49th AIAA Aerospace Sciences Meeting including the New Horizons Forum and Aerospace Exposition, Jan. 2011.
[17]. Gaurav Gupta, Erik Fernandez, Marcel Otto, Jayanta S. Kapat, "Experimental and numerical investigation of fully turbulent flow in a rectangular channel with dimples and protrusions," AIAA Propulsion and Energy 2019 Forum, Sep. 2019.
[18]. Yadav R, Bodavula A, "Numerical investigation of the effect of triangular cavity on the unsteady aerodynamics of NACA 0012 at a low Reynolds number," Proceedings of the Institution of Mechanical Engineers, Part G: Journal of Aerospace Engineering, vol. 236, no. 6, pp. 1064-1080, June 2021.
[19]. Bodavula A, Yadav R, and Guven U, "Numerical investigation of the unsteady aerodynamics of NACA 0012 with suction surface protrusion," Aircraft Engineering and Aerospace Technology, vol. 92, no. 2, pp. 186-200, Jan. 2020.
[20]. Bodavula A, Yadav R, Guven U, "Stall Mitigation and Lift Enhancement of NACA 0012 with Triangle-Shaped Surface Protrusion at a Reynolds Number of 105," SAE Int. J. Aerosp, vol. 12, no. 2, pp. 133-151, Nov. 2019.
[21]. Patial S, Jain P, Rawat P, Bodavula A, and Yadav R, "The study of the effect of the cavity on the flow over NACA 0012 and Selig 7003 aerofoil at Low Reynolds number using Vortex Shading Method," AIAA 2020-2218. AIAA Scitech 2020 Forum, Jan. 2020.
[22]. Bodavula A, Yadav R, "Numerical investigation of the effect of the spanwise groove on the aerodynamic characteristic of a NACA 0012 airfoil using γ-Reθt transition turbulence model," International Journal of Fluid Mechanics Research, vol. 49, no. 6, pp. 1-17, Jan. 2022.
[23]. Bodavula Aslesha, "Effect of surface protrusions and cavities on airfoil aerodynamic efficiency at low Reynolds number," Diss. College of Engineering, UPES, Sep. 2020.
[24]. Lodefier K, Merci B, De Langhe C, and Dick E, "Transition modeling with the SST turbulence model and intermittency transport equation," ASME Paper, June 2003.
[25]. Langtry R. B., and Menter F. R, "Correlation-based transition modeling for unstructured parallelized computational fluid dynamics codes," AIAA Journal vol. 47, no. 12, pp. 2894–2906, Dec. 2009.
[26]. Menter F. R, "Two-equation eddy-viscosity turbulence models for engineering applications," AIAA Journal, vol. 32, no. 8, pp. 1598–1605, Aug. 1994.
[27]. Van Ingen J. L, "The eN method for transition prediction: historical review of work at TU delft," 38th Fluid Dynamics Conference and Exhibit, AIAA Paper, June 2008.

DOI: https://doi.org/10.15379/ijmst.v10i4.2256